Aerosol Research Letter

Aerosol Imaging with a Soft X-Ray Free Electron Laser

Michael J. Bogan,[1,2] Sébastien Boutet,[1] Henry N. Chapman,[3,4] Stefano Marchesini,[5] Anton Barty,[2] W. Henry Benner,[2] Urs Rohner,[2,6] Matthias Frank,[2] Stefan P. Hau-Riege,[2] Sasa Bajt,[3] Bruce Woods,[2] M. Marvin Seibert,[7] Bianca Iwan,[7] Nicusor Timneanu,[7] Janos Hajdu,[7] and Joachim Schulz[3]

[1]*SLAC National Accelerator Laboratory, Menlo Park, California, USA*
[2]*Lawrence Livermore National Laboratory, Livermore California, USA*
[3]*Deutsches Elektronen-Synchrotron DESY, Notkestraße 85, Hamburg, Germany*
[4]*Universität Hamburg, Luruper Chaussee 149, Hamburg, Germany*
[5]*Lawrence Berkeley National Laboratory, Berkeley, California, USA*
[6]*TOFWERK AG, Uttigenstrasse 22, Thun, Switzerland*
[7]*Uppsala University, Husargatan 3, Uppsala, Sweden*

Lasers have long played a critical role in the advancement of aerosol science. A new regime of ultrafast laser technology has recently be realized, the world's first soft x-ray free electron laser. The Free electron LASer in Hamburg, FLASH, user facility produces a steady source of 10 femtosecond pulses of 7–32 nm x-rays with 10^{12} photons per pulse. The high brightness, short wavelength, and high repetition rate (>500 pulses per second) of this laser offers unique capabilities for aerosol characterization. Here we use FLASH to perform the highest resolution imaging of single PM2.5 aerosol particles in flight to date. We resolve to 35 nm the morphology of fibrous and aggregated spherical carbonaceous nanoparticles that existed for less than two milliseconds in vacuum. Our result opens the possibility for high spatial- and time-resolved single particle aerosol dynamics studies, filling a critical technological need in aerosol science.

Received 9 August 2009; accepted 31 October 2009.

Special thanks are due to the scientific and technical staff of the FLASH at DESY, Hamburg, in particular to R. Treusch, J. Schneider, S. Dusterer, T. Tschentscher, J. Feldhaus, R. L. Johnson, U. Hahn, T. Nunez, K. Tiedtke, S. Toleikis, E. L. Saldin, E. A. Schneidmiller, and M. V. Yurkov. We are grateful to our collaborators in T. Moller's group at Technische Universitat Berlin for accommodating our experiment in their vacuum chamber. This work was supported by the following agencies: The U.S. Department of Energy by Lawrence Livermore National Laboratory in part under Contract W-7405-Eng-48 and in part under Contract DE-AC52-07NA27344, Lawrence Livermore National Laboratory (the project 05-SI-003 from the Laboratory Directed Research and Development Program of LLNL); the U.S. Department of Energy by the SLAC National Accelerator Laboratory in part under contract number DE-AC02-76SF00515; the Deutsches Elektronen-Synchrotron, a research center of the Helmholtz Association. Additional support comes from the DFG Cluster of Excellence at the Munich Centre for Advanced Photonics (www.munich-photonics.de), from the Virtual Institute Program of the Helmholtz Society, and by the Swedish Research Council.

Address correspondence to Michael J. Bogan, Stanford PULSE Institute for Ultrafast Energy Science, SLAC National Accelerator Laboratory, 2575 Sand Hill Road MS59, Menlo Park, CA 94025, USA. E-mail: mbogan@slac.stanford.edu

[Supplementary materials are available for this article. Go to the publisher's online edition of *Aerosol Science and Technology* to view the free supplementary files.]

Nanoscale morphology is a principal factor that helps define chemical reactivity, aerodynamic transport, aggregation, and optical properties of airborne particulate matter (PM) (Ramanathan and Carmichael 2008; Zhang et al. 2008). Of particular interest recently is PM of $\leq$2.5 μm in mobility diameter (PM2.5). In the form of black carbon cenospheres in soot, it represents the second most dominant contribution to current global warming (Ramanathan and Carmichael 2008). PM2.5 efficiently transports into the human lung and experience with asbestos fibers has even shown that nanoscale morphology of PM2.5 alone can determine toxicity (Mossman et al. 1990). The primary tool for imaging PM morphology, electron microscopy (EM), requires particle capture onto a substrate, a step that removes the aerosol from its natural environment, the air, and places it on a solid support, the EM grid. Thus, EM cannot follow dynamics of airborne single particle morphology. *In situ* sampling and characterization techniques such as differential mobility analysis (Virtanen et al. 2004; Zhang et al. 2008) enable aerodynamic diameter measurements of aerosols but can only be correlated with off-line imaging methods such as EM. Analysis of particulate matter in flight using synchrotron-based x-ray sources is a promising development but is limited to ensemble measurements (Beaucage et al. 2004; Shu et al. 2005; Shu et al. 2006).

Work supported in part by US Department of Energy contract DE-AC02-76SF00515.

X-ray tomographic microscopy can probe the 3D structure of individual inorganic nanoparticles on a substrate (Chapman et al. 2006b; Miao et al. 2006; Zahiri et al. 2008) but many aerosols are composed of radiation sensitive soft matter, limiting the resolution due to the long x-ray exposure time necessary as observed in biological imaging (Shapiro et al. 2005). Moreover, when applied to aerosols this method also requires transfer of the particles from air to a solid support. In its current state, knowledge of PM2.5 morphology and dynamics gained from airborne single particle measurements is incomplete, requiring a completely new approach to determine key relationships between morphology, mobility, aggregation, catalytic properties, and light scattering (Friedlander and Pui 2004).

These limitations in the analysis of PM can now be overcome by the realization of the first ultrafast soft x-ray free-electron-laser, FLASH (Ackermann et al. 2007), and the demonstration of its use for femtosecond diffractive imaging beyond the damage limit (Chapman 2009; Chapman et al. 2006a). Iterative transform phase retrieval techniques (Fienup 1982; Marchesini 2007) enable direct imaging of individual particles illuminated by soft x-ray FLASH pulses using the resultant diffraction pattern alone. (Bogan et al. 2008). The reconstructed electron density is essentially a 2D image qualitatively similar to electron microscopy images used to measure PM2.5 morphology (Dye et al. 2000). Previous imaging experiments at FLASH were limited in resolution to about 60 nm by the scattering geometry and the use of wavelengths longer than 13 nm (Bogan et al. 2008). For these studies on PM2.5 in flight, we extended the resolution of single particle diffractive imaging to 35 nm by capturing single-shot 2D images of PM2.5 in flight using 7 nm FLASH pulses. We also apply shape analysis methods used in electron microscopy to interpret the particle morphology from the reconstructed electron density. Two types of PM2.5 with complex morphology were investigated: aggregates of spherical polystyrene nanoparticles (carbon cenosphere analogues) and dry powder-dispersed carbon nanofibers (asbestos fiber analogues).

Figure 1 shows a schematic of the ultrafast single shot x-ray diffraction experiment used to image PM2.5. To begin, we calibrated our soft x-ray camera (Bajt et al. 2008) with a test aerosol of polystyrene spheres of known size generated by electrospraying a dilute suspension of the particles. The aerosol is delivered into the x-rays using a differentially pumped aerodynamic lens stack (Benner et al. 2008; Bogan et al. 2008). Upon coincident arrival of a particle and x-ray pulse with camera readout, the pattern of diffracted photons was recorded. Convenient separation between sample and detector ensures appropriate sampling of the angular diffraction distribution. In this lensless diffraction geometry the image resolution is defined in principle by the maximum momentum transfer recorded, while the image field of view, and hence the maximum size of the object that can be studied, is inversely proportional to the angular sampling period of the detector. The detector angular extent to reach 20 nm resolution can be achieved with a very convenient separation between sample and detector of 5 cm, and the 2048 × 2048 pixels

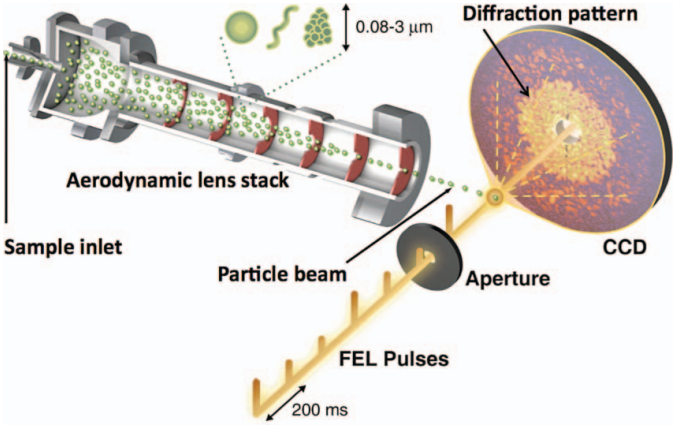

FIG. 1. FLASH diffraction of aerosols in situ. Aerosols delivered through a differentially pumped aerodynamic lens stack are converted into a particle beam that is steered into the x-ray interaction region. FLASH is operated at 5 Hz in multi-bunch mode with 100 pulses per bunch separated by 10 μs. Upon coincident arrival of a particle and X-ray pulse with readout of an X-ray sensitive area detector, a diffraction pattern containing particle structural information is recorded.

of the detector allows us to image objects up to 20 micron in size. For the test aerosol of spheres, radial averages match Mie theory calculations (line) of scattering from injected spheres with 88, 140, and 194 nm diameter collected with FLASH operating at 13.5 nm (Figure 2).

The morphology of test aerosols can be influenced by the method used to generate them. A nebulizer generating 0.7–4 μm droplets was used to aerosolize a suspension of 250 nm diameter spherical polystyrene nanoparticles in 25 mM ammonium acetate. In contrast to the approximately 200 nm diameter primary droplets of the electrospray source, the nebulized droplets are large enough to contain multiple spheres. After the volatile solvent evaporates from a nebulized droplet, the resultant dry particle is typically an aggregate comprised of multiple spheres. Example diffraction patterns collected from a single 250 nm diameter sphere and aggregates with N = 2, 3, and 4 components are shown in Figure 3, top row. The coherent illumination of multiple spheres results in interference fringes that encode the number of spheres in the aggregate, their relative orientation to each other and orientation of the aggregate to the x-ray pulse. The electron density of each aggregate was reconstructed to 35 nm resolution using iterative phase retrieval with the ESPRESSO algorithm, arXiv:0809.2006v1 (Figure 3, bottom row).

As N increases, increasingly complex coherent speckles modulate the scattered signal. As with the simpler fringe patterns from few-component aggregates the diffraction pattern encodes the locations of the spheres in the aggregate. For example, Figure 4a shows a diffraction pattern collected from a large aggregate of 88 nm spheres. Travelling through vacuum at about 150 m/s, this aggregate particle was unique and existed for less than two milliseconds after exiting the aerodynamic lens stack. Based on previous time-resolved x-ray diffractive

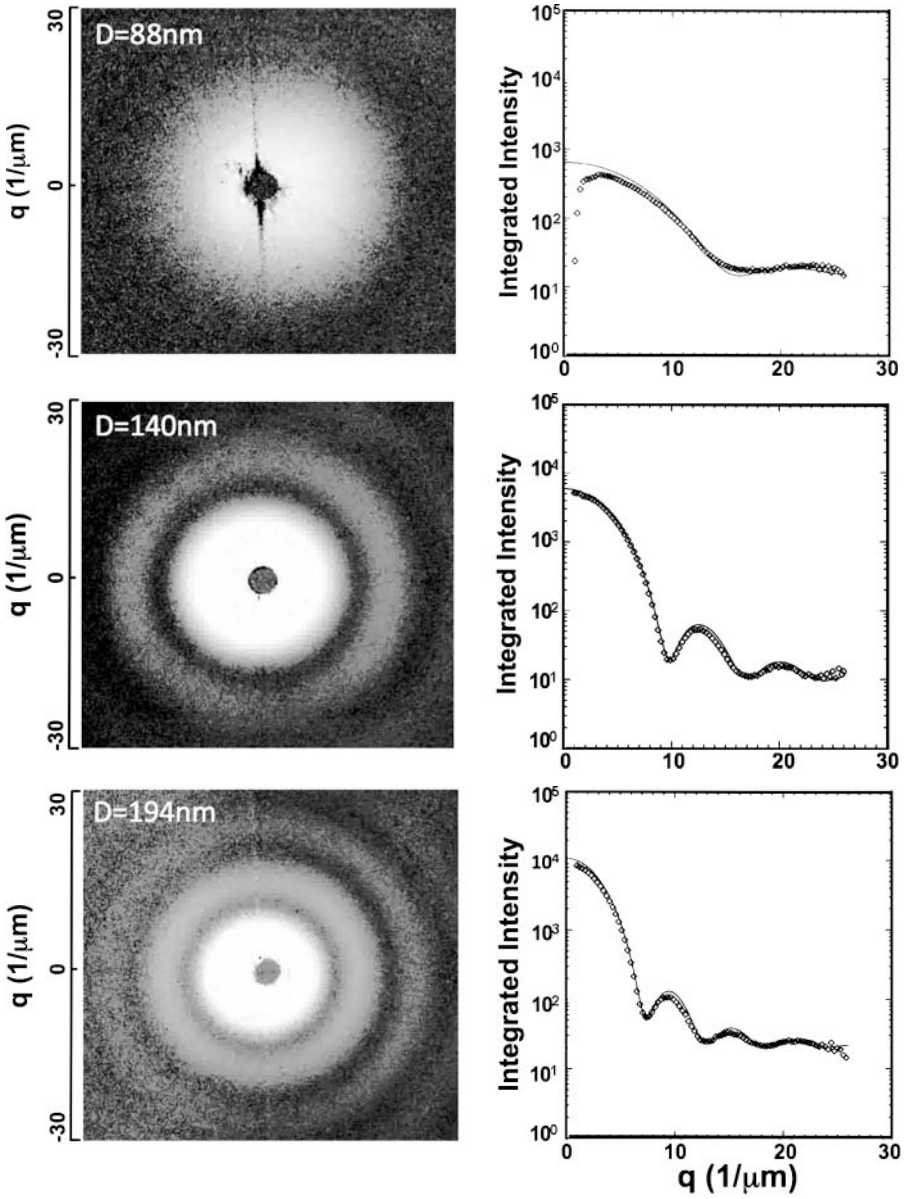

FIG. 2. FLASH diffraction patterns of single spheres and plots of corresponding radial averages (dots) collected while injecting 88 nm, 140 nm, and 194 nm diameter spherical polystyrene particles into the x-rays. Radial averages match Mie theory calculations (line) of scattering from spheres with injected particle diameters.

imaging experiments (Chapman et al. 2007), the particle was completely destroyed just picoseconds after the x-ray pulse interacted with the particle. Thus, its 3D structure cannot be obtained by proposed methods for diffraction patterns collected from identical objects (Huldt et al. 2003). Potential exists to extract additional degrees of morphological information from unique particles in flight using proposed tomographic femtosecond diffractive imaging methods (Schmidt et al. 2008), but these are currently unavailable. Here we focus on the information that can be extracted from this single-shot diffraction pattern of a unique object by applying morphological analysis methods utilized in electron microscopy to the reconstructed electron density.

Fractal dimensions or other measures of complex particle shape such as convexity, circularity, or elongation are typically used when PM2.5 morphology is characterized by EM (Dye et al. 2000). For FLASH diffractive imaging of aerosols, the reconstructed electron density (Figure 4b) is converted to a binary image and the particle's circularity, convexity and elongation is calculated. The circularity ratio is a compactness measure assigned a value between 0 and 1. It is defined as the area of the shape of the particle to the area of a circle with the same

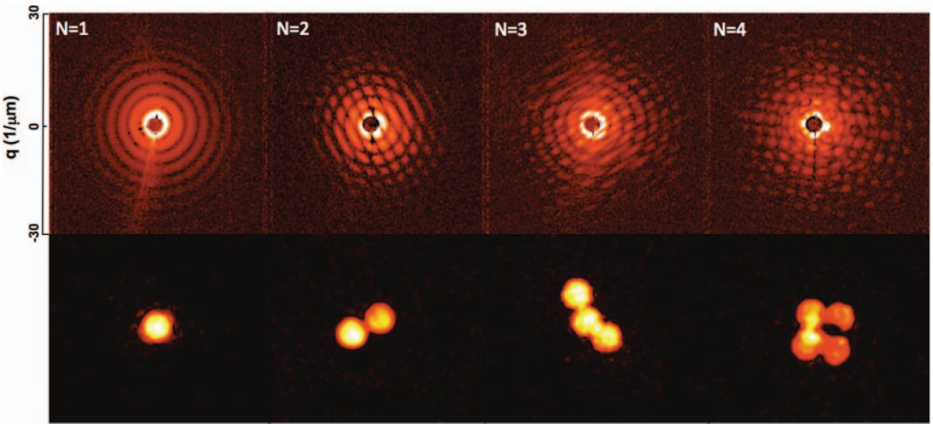

FIG. 3. FLASH diffraction patterns of single and aggregated 250 nm diameter spheres, where N equals the number of particles in the aggregate. The bottom row shows images of reconstructed electron density that were solved using ESPRESSO (arXiv:0809.2006v1).

perimeter as the particle shape. For a circle, the ratio is one; for a square, it is $\pi/4$; for an infinitely long and narrow shape, it is zero. Elongation is a measure of the particle aspect ratio and is defined as 1-W/L, where W is particle width and L is particle length. Convexity measures particle roughness by dividing the convex hull perimeter (the red line surrounding the particle in Figure 4c) by the particle perimeter. Calculated parameters for the aggregate particle are listed in Figure 4c.

A second type of particle, a carbon nanofiber about 700 nm long, was also imaged. To deliver these particles into the x-rays, a dry powder of carbon nanofibers was entrained into a two liter per minute (lpm) air flow using a shaker-system upstream of the aerodynamic lens stack, similar to the method (Bon Ki et al. 2006) used for tandem mobility mass anlaysis. Figures 4d and e show the single-shot diffraction pattern and the corresponding image of the nanofiber. To increase confidence that the recovered images are correct and unique the phase-retrieval process was repeated using 500 random starts. The repeatability of the recovered images as a function of resolution measures the effective phase-retrieval transfer function (PRTF). The

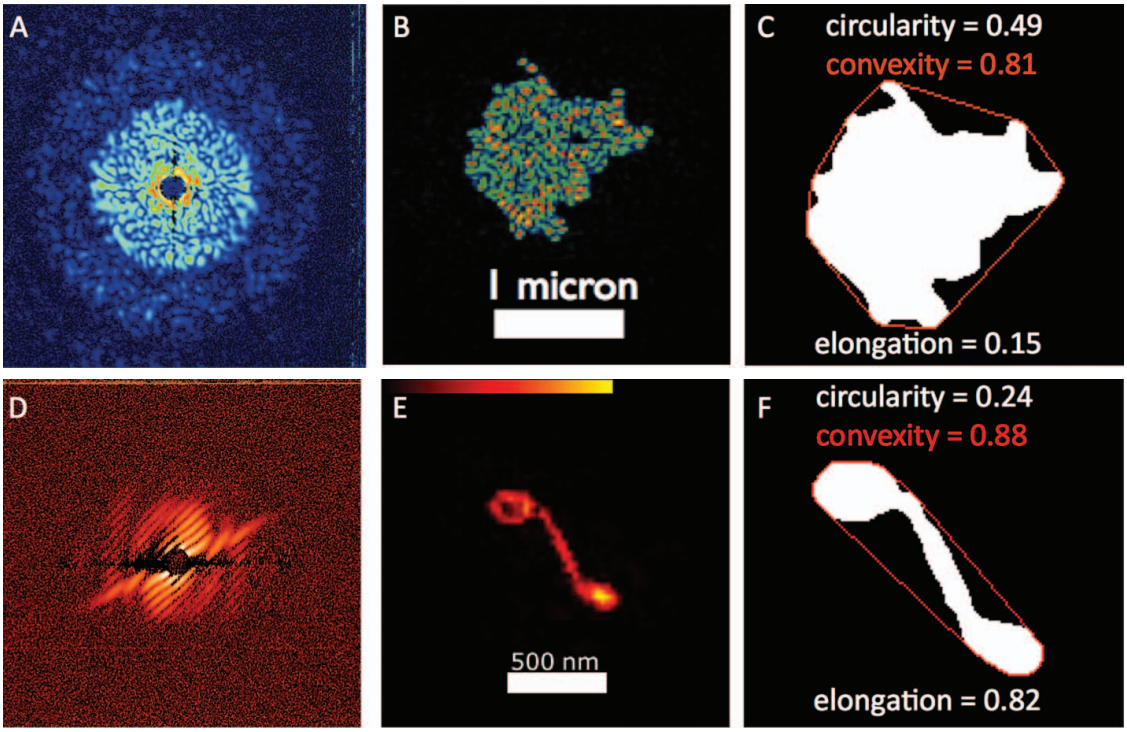

FIG. 4. FLASH diffractive imaging of PM2.5 morphology. The diffraction pattern (left), reconstructed electron density (middle), and binary convex hull image (right) of an aggregate particle comprised of 88 nm spheres (top row) and a single carbon nanofiber (bottom row).

half-period resolution of the PRTF is commonly quoted as the resolution of the reconstructed image, in this case 35 nm (see supplemental information). Calculated parameters from the shape analysis are shown in Figure 4f. The combination of single-shot x-ray diffraction with morphological interpretation of the reconstructed electron density shows that the nanofiber is of similar roughness, less circular, and more elongated than the aggregate particle. No other method exists for performing such a direct imaging comparison of PM2.5 nanoscale morphology from aerosols in flight.

We have reported the highest-resolution images of airborne PM2.5 ever recorded.FLASH diffractive imaging of aerosols in flight provides high-resolution morphological information on single particles that have not been modified by capture on a substrate. The approach complements EM studies but has sample penetration depth advantages inherent to x-rays. Subnanometer resolution has been predicted for single-shot diffractive imaging using hard x-ray lasers (Bergh et al. 2008), suggesting that even higher-resolution aerosol dynamics studies required to solve challenges in particulate inhalation-induced genetic damage (Baccarelli et al. 2009), inhalable pharmaceuticals (Groneberg et al. 2003), black carbon influence on global climate (Ramanathan and Carmichael 2008), and even accretion in protoplanetary discs (Throop et al. 2001) can be addressed in the future. A FLASH upgrade is expected to enable lasing at 4.5 nm in 2010, and early commissioning experiments have already begun at the Linac Coherent Light Source, which is lasing at 0.15 nm. Exploration of the limit of detection for morphological determination with hard x-ray FELs is warranted. Such studies would provide empirical values for the number of scattered photons from well-defined materials, information critical to simulations of the determination of biological structure by single particle diffractive imaging. Based on our previous work with fixed target samples (Barty et al. 2008; Chapman et al. 2007), measurements of dynamical processes in single particles initiated by ultrafast laser pulses will be a worthwhile extension of single particle diffractive imaging.

REFERENCES

Ackermann, W., Asova, G., Ayvazyan, V., Azima, A., Baboi, N., Bahr, J., Balandin, V., Beutner, B., Brandt, A., Bolzmann, A., Brinkmann, R., Brovko, O. I., Castellano, M., Castro, P., Catani, L., Chiadroni, E., Choroba, S., Cianchi, A., Costello, J. T., Cubaynes, D., Dardis, J., Decking, W., Delsim Hashemi, H., Delserieys, A., Di Pirro, G., Dohlus, M., Dusterer, S., Eckhardt, A., Edwards, H. T., Faatz, B., Feldhaus, J., Flottmann, K., Frisch, J., Frohlich, L., Garvey, T., Gensch, U., Gerth, C., Gorler, M., Golubeva, N., Grabosch, H. J., Grecki, M., Grimm, O., Hacker, K., Hahn, U., Han, J. H., Honkavaara, K., Hott, T., Huning, M., Ivanisenko, Y., Jaeschke, E., Jalmuzna, W., Jezynski, T., Kammering, R., Katalev, V., Kavanagh, K., Kennedy, E. T., Khodyachykh, S., Klose, K., Kocharyan, V., Korfer, M., Kollewe, M., Koprek, W., Korepanov, S., Kostin, D., Krassilnikov, M., Kube, G., Kuhlmann, M., Lewis, C. L. S., Lilje, L., Limberg, T., Lipka, D., Lohl, F., Luna, H., Luong, M., Martins, M., Meyer, M., Michelato, P., Miltchev, V., Moller, W. D., Monaco, L., Muller, W. F. O., Napieralski, O., Napoly, O., Nicolosi, P., Nolle, D., Nunez, T., Oppelt, A., Pagani, C., Paparella, R., Pchalek, N., Pedregosa Gutierrez, J., Petersen, B., Petrosyan, B., Petrosyan, G., Petrosyan, L., Pfluger, J., Plonjes, E., Poletto, L., Pozniak, K., Prat, E., Proch, D., Pucyk, P., Radcliffe, P., Redlin, H., Rehlich, K., Richter, M., Roehrs, M., Roensch, J., Romaniuk, R., Ross, M., Rossbach, J., Rybnikov, V., Sachwitz, M., Saldin, E. L., Sandner, W., Schlarb, H., Schmidt, B., Schmitz, M., Schmuser, P., Schneider, J. R., Schneidmiller, E. A., Schnepp, S., Schreiber, S., Seide, I. M., Sertore, D., Shabunov, A. V., Simon, C., Simrock, S., Sombrowski, E., Sorokin, A. A., Spanknebel, P., Spesyvtsev, R., Staykov, L., Steffen, B., Stephan, F., Stulle, F., Thom, H., Tiedtke, K., Tischer, M., Toleikis, S., Treusch, R., Trines, D., Tsakov, I., Vogel, E., Weiland, T., Weise, H., Wellhofer, M., Wendt, M., Will, I., Winter, A., Wittenburg, K., Wurth, W., Yeates, P., Yurkov, M. V., Zagorodnov, I., and Zapfe, K. (2007). Operation of a Free-Electron Laser from the Extreme Ultraviolet to the Water Window. *Nat. Photonics* 1:336–342.

Baccarelli, A., Wright, R. O., Bollati, V., Tarantini, L., Litonjua, A. A., Suh, H. H., Zanobetti, A., Sparrow, D., Vokonas, P. S., and Schwartz, J. (2009). Rapid DNA Methylation Changes after Exposure to Traffic Particles. *Am. J. Respir. Crit. Care Med.* 179:572–578.

Bajt, S., Chapman, H. N., Spiller, E., Alameda, J., Woods, B. W., Frank, M., Bogan, M. J., Barty, A., Boutet, S., Marchesini, S., Hau-Riege, S. P., Hajdu, J., and Shapiro, D. (2008). A Camera for Coherent Diffractive Imaging and Holography with a Soft-X-Ray Free Electron Laser. *Appl. Opt.* 47:1673–1683.

Barty, A., Boutet, S., Bogan, M. J., Hau-Riege, S., Marchesini, S., Sokolowski-Tinten, K., Stojanovic, N., Tobey, R., Ehrke, H., Cavalleri, A., Dusterer, S., Frank, M., Bajt, S., Woods, B. W., Seibert, M. M., Hajdu, J., Treusch, R., and Chapman, H. N. (2008). Ultrafast Single-Shot Diffraction Imaging of Nanoscale Dynamics. *Nat. Photonics* 2:415–419.

Beaucage, G., Kammler, H. K., Mueller, R., Strobel, R., Agashe, N., Pratsinis, S. E., and Narayanan, T. (2004). Probing the Dynamics of Nanoparticle Growth in a Flame Using Synchrotron Radiation. *Nat. Materials* 3:370–374.

Benner, W. H., Bogan, M. J., Rohner, U., Boutet, S., Woods, B., and Frank, M. (2008). Non-Destructive Characterization and Alignment of Aerodynamically Focused Particle Beams Using Single Particle Charge Detection. *J. Aerosol Sci.* 39:917–928.

Bergh, M., Huldt, G., Timneanu, N., Maia, F. R. N. C., and Hajdu, J. (2008). Feasibility of Imaging Living Cells at Subnanometer Resolutions by Ultrafast X-Ray Diffraction. *Quar. Rev. Biophys.* 41:181–204.

Bogan, M. J., Benner, W. H., Boutet, S., Rohner, U., Frank, M., Barty, A., Seibert, M. M., Maia, F. R. N. C., Marchesini, S., Bajt, S., Woods, B. W., Riot, V., Hau-Riege, S. P., Marklund, E., Spiller, E., Svenda, M., Hajdu, J., and Chapman, H. N. (2008). Single Particle X-Ray Diffractive Imaging. *Nano. Lett.* 8:310–316.

Bon Ki, K., Mark, S. E., Andrew, D. M., Mark, R. S., and Peter, H. M. (2006). In Situ Structure Characterization of Airborne Carbon Nanofibres by a Tandem Mobility-Mass Analysis. *Nanotechnology*:3613.

Chapman, H. N. (2009). X-Ray Imaging Beyond the Limits. *Nat. Materials* 8:299–301.

Chapman, H. N., Barty, A., Bogan, M. J., Boutet, S., Frank, M., Hau-Riege, S. P., Marchesini, S., Woods, B. W., Bajt, S., Benner, W. H., London, R. A., Plonjes, E., Kuhlmann, M., Treusch, R., Dusterer, S., Tschentscher, T., Schneider, J. R., Spiller, E., Moller, T., Bostedt, C., Hoener, M., Shapiro, D. A., Hodgson, K. O., van der Spoel, D., Burmeister, F., Bergh, M., Caleman, C., Huldt, G., Seibert, M. M., Maia, F. R. N. C., Lee, R. W., Szoke, A., Timneanu, N., and Hajdu, J. (2006a). Femtosecond Diffractive Imaging with a Soft-X-Ray Free-Electron Laser. *Nat. Physics* 2:839–843.

Chapman, H. N., Barty, A., Marchesini, S., Noy, A., Hau-Riege, S. P., Cui, C., Howells, M. R., Rosen, R., He, H., Spence, J. C. H., Weierstall, U., Beetz, T., Jacobsen, C., and Shapiro, D. (2006b). High-Resolution Ab Initio Three-Dimensional X-Ray Diffraction Microscopy. *J. Opt. Soc. Amer. A* 23:1179–1200.

Chapman, H. N., Hau-Riege, S. P., Bogan, M. J., Bajt, S., Barty, A., Boutet, S., Marchesini, S., Frank, M., Woods, B. W., Benner, W. H., London, R. A., Rohner, U., Szoke, A., Spiller, E., Moller, T., Bostedt, C., Shapiro, D., Kuhlmann, M., Treusch, R., Plonjes, E., Burmeister, F., Bergh, M., Caleman,

C., Huldt, G., Seibert, M. M., and Hajdu, J. (2007). Femtosecond Time-Delay X-Ray Holography. *Nature* 448:676–679.

Dye, A. L., Rhead, M. M., and Trier, C. J. (2000). The Quantitative Morphology of Roadside and Background Urban Aerosol in Plymouth, UK. *Atmos. Env.* 34:3139–3148.

Fienup, J. R. (1982). A Phase Retreival Algorithms—A Comparison. *Appl. Opt.* 21:2758–2769.

Friedlander, S. K., and Pui, D. Y. H. (2004). Emerging Issues in Nanoparticle Science and Technology. *J. Nanoparticle Res.* 6:313–320.

Groneberg, D. A., Witt, C., Wagner, U., Chung, K. F., and Fischer, A. (2003). Fundamentals of Pulmonary Drug Delivery. *Respir. Med.* 97:382–387.

Huldt, G., Szoke, A., and Hajdu, J. (2003). Diffraction Imaging of Single Particles and Biomolecules. *J. Struct. Biol.* 144:219–227.

Marchesini, S. (2007). A Unified Evaluation of Iterative Projection Algorithms for Phase Retrieval. *Rev. Sci. Inst.* 78:011301.

Miao, J., Chen, C.-C., Song, C., Nishino, Y., Kohmura, Y., Ishikawa, T., Ramunno-Johnson, D., Lee, T.-K., and Risbud, S. H. (2006). Three-Dimensional GaN-Ga_2O_3 Core Shell Structure Revealed by X-Ray Diffraction Microscopy. *Phys. Rev. Lett.* 97:215503–215504.

Mossman, B. T., Bignon, J., Corn, M., Seaton, A., and Gee, J. B. (1990). Asbestos: Scientific Developments and Implications for Public Policy. *Science* 247:294–301.

Ramanathan, V., and Carmichael, G. (2008). Global and Regional Climate Changes Due to Black Carbon. *Nat. Geosci.* 1:221–227.

Schmidt, K. E., Spence, J. C. H., Weierstall, U., Kirian, R., Wang, X., Starodub, D., Chapman, H. N., Howells, M. R., and Doak, R. B. (2008). Tomographic Femtosecond X-Ray Diffractive Imaging. *Phys. Rev. Lett.* 101:115507–115504.

Shapiro, D., Thibault, P., Beetz, T., Elser, V., Howells, M. R., Jacobsen, C., Kirz, J., Lima, E., Miao, H., Neiman, A. M., and Sayre, D. (2005). Biological Imaging by Soft X-Ray Diffraction Microscopy. *Proc. Natl. Acad. Sci.* 102:15343.

Shu, J., Wilson, K., Arrowsmith, A. N., Ahmed, M., and Leone, S. R. (2005). Light Scattering of Ultrafine Silica Particles by VUV Synchrotron Radiation. *Nano. Lett.* 5:1009–1015.

Shu, J., Wilson, K. R., Ahmed, M., Leone, S. R., Graf, C., and Ruhl, E. (2006). Elastic Light Scattering From Nanoparticles by Monochromatic Vacuum-Ultraviolet Radiation. *J. Chem. Phys.* 124:034707–034709.

Throop, H. B., Bally, J., Esposito, L. W., and McCaughrean, M. J. (2001). Evidence for Dust Grain Growth in Young Circumstellar Disks. *Science* 292:1686–1689.

Virtanen, A. K. K., Ristimaki, J. M., Vaaraslahti, K. M., and Keskinen, J. (2004). Effect of Engine Load on Diesel Soot Particles. *Env. Sci. Tech.* 38:2551–2556.

Zahiri, S. H., Mayo, S. C., and Jahedi, M. (2008). Characterization of Cold Spray Titanium Deposits by X-Ray Microscopy and Microtomography. *Microscopy and Microanalysis* 14:260–266.

Zhang, R., Khalizov, A. F., Pagels, J., Zhang, D., Xue, H., and McMurry, P. H. (2008). Variability in Morphology, Hygroscopicity, and Optical Properties of Soot Aerosols During Atmospheric Processing. *Proc. Natl. Acad. Sci.* 105:10291–10296.